

RESEARCH ARTICLE | SEPTEMBER 20 2023

Three-dimensional printed microcantilever with mechanical metamaterial for fiber-optic microforce sensing

Famei Wang ; Mengqiang Zou ; Changrui Liao  ; Bozhe Li; Dejun Liu ; Jie Zhou; Haoqiang Huang ; Jinlai Zhao ; Chao Liu; Paul K. Chu ; Yiping Wang

 Check for updates

APL Photonics 8, 096108 (2023)

<https://doi.org/10.1063/5.0159706>



View Online



Export Citation

CrossMark

Articles You May Be Interested In

A functional integral formalism for quantum spin systems

J. Math. Phys. (July 2008)

Modes selection in polymer mixtures undergoing phase separation by photochemical reactions

Chaos (June 1999)

Spreading of a surfactant monolayer on a thin liquid film: Onset and evolution of digitated structures

Chaos (March 1999)



yttrium iron garnet, zeolites, nano ribbons, epitaxial crystal growth, cerium oxide polishing powder, surface functionalized nanoparticles, sapphire windows, Nd:YAG, spintronics, raman substrates, silver nanoparticles, perovskites, MOCVD, beta-barium borate, rare earth metals, quantum dots, osmium, scintillation Ce:YAG, refractory metals, laser crystals, anodic aluminum oxide, niobate, InAs wafers, MOFs, AuNPs, ZnS, CdTe, perovskite crystals, transparent ceramics

glassy carbon, III-IV semiconductors, gallium lump, copper nanoparticles, organometallics, europium phosphors, photonics, infrared dyes, ultra high purity materials, transparent ceramics, CIGS, cermet, nanodispersions, MBE grade materials, thin film, OLED lighting, solar energy, sputtering targets, fiber optics, h-BN, deposition slugs, CVD precursors, photovoltaics, metamaterials, borosilicate glass, YBCO superconductors, InGaAs, indium tin oxide, MgF2, rutile, diamond micropowder, optical glass

Beamsplitters, fused quartz, additive manufacturing



Now Invent.™

www.americanelements.com

© 2001-2022, American Elements LLC, a U.S. Registered Trademark.

The Next Generation of Material Science Catalogs

Three-dimensional printed microcantilever with mechanical metamaterial for fiber-optic microforce sensing



Cite as: APL Photon. 8, 096108 (2023); doi: 10.1063/5.0159706
Submitted: 25 May 2023 • Accepted: 18 August 2023 •
Published Online: 20 September 2023



Famei Wang,^{1,2} Mengqiang Zou,^{1,2} Changrui Liao,^{1,2,a)} Bozhe Li,^{1,2} Dejun Liu,^{1,2} Jie Zhou,^{1,2} Haoqiang Huang,^{1,2} Jinlai Zhao,³ Chao Liu,⁴ Paul K. Chu,⁵ and Yiping Wang^{1,2}

AFFILIATIONS

¹ Shenzhen Key Laboratory of Ultrafast Laser Micro/Nano Manufacturing, Key Laboratory of Optoelectronic Devices and Systems of Ministry of Education/Guangdong Province, College of Physics and Optoelectronic Engineering, Shenzhen University, Shenzhen 518060, China

² Shenzhen Key Laboratory of Photonic Devices and Sensing Systems for Internet of Things, Guangdong and Hong Kong Joint Research Centre for Optical Fibre Sensors, State Key Laboratory of Radio Frequency Heterogeneous Integration, Shenzhen University, Shenzhen 518060, China

³ College of Materials Science and Engineering, Shenzhen Key Laboratory of Polymer Science and Technology, Guangdong Research Center for Interfacial Engineering of Functional Materials, Shenzhen 518060, China

⁴ School of Electronics Science, Northeast Petroleum University, Daqing 163318, China

⁵ Department of Physics, Department of Materials Science and Engineering, and Department of Biomedical Engineering, City University of Hong Kong, Tat Chee Avenue, Kowloon, Hong Kong, China

Note: This paper is part of the APL Photonics Special Topic on Ultrafast Laser Fabrication Enabled Photonics and Devices.

^{a)} Author to whom correspondence should be addressed: cliao@szu.edu.cn

ABSTRACT

Mechanical metamaterials can adjust mechanical properties of structures flexibly through a mechanical structural design based on the premise that the materials remain unchanged. Here, a cantilever probe microstructure is designed using mechanical metamaterials for an optical fiber microforce sensor tip that can be prepared by femtosecond laser-induced two-photon polymerization. The elastic constant k of the fabricated fiber-optic microforce sensor has been adjusted by two orders of magnitude from 0.165 to 46 N/m, and the geometric configuration of the cantilever beam can be tailored to match the mechanical properties of biological specimens. This fiber microforce sensor shows an ultra-high force sensitivity of 154 nm/ μ N and a force resolution of up to 130 pN. The optical fiber microforce sensor that shows the lowest force resolution in a direct-contact mode has high potential for biosensing applications, and the results reveal a potential design strategy for special scanning tunneling microscope probes with unique physical properties.

© 2023 Author(s). All article content, except where otherwise noted, is licensed under a Creative Commons Attribution (CC BY) license (<http://creativecommons.org/licenses/by/4.0/>). <https://doi.org/10.1063/5.0159706>

I. INTRODUCTION

Detection of micro–nano-force is important in many fields, including biomedicine,^{1–4} cytology,^{5–7} molecular chemistry,⁸ genetics (DNA),⁹ environmental detection (detection of bacteria),¹⁰ food industry (detection of micro-organisms),¹¹ nanoscale manufacturing,^{12–14} and other fields. The commonly used micro-electromechanical systems (MEMS) microforce sensors are badly

affected by the large demodulation systems required, low detection sensitivity, and poor electromagnetic compatibility. In this respect, optical fiber sensors offer advantages that include stable operation, small size, high sensitivity, and resistance to electromagnetic interference.^{15–18} It is also important to use optical fibers to replace the complex and huge optical path space required for the conventional sensors to reduce the device size. As a highly sensitive MEMS device, the microcantilever boasts no labeling requirements,

real-time operation, precise positioning, and specific detection capabilities, and the optical fiber Fabry–Pérot interferometer (FPI) sensor configuration consisting of a microcantilever has garnered considerable research interest.^{19–22} The most direct way to integrate a microcantilever beam with an optical fiber is to connect a commercial microcantilever beam probe to the optical fiber end face. Although microcantilever beams with various shapes that are made from different materials can be integrated into the optical fiber end face, each cantilever beam must be aligned accurately to the fiber end face using high-precision instruments and fixed with adhesives, consequently compromising the repeatability and the stability of the resulting sensor.

Optical fiber integrated microcantilever systems have been prepared by picosecond and femtosecond laser ablation techniques,^{23–25} focused ion beam processing,²⁶ and other methods.^{27–29} Because of the limited machining accuracy of these techniques, rough and thick surfaces are produced on the cantilever by picosecond laser ablation and stress sensing based on cantilever deformation is then affected by the surface quality. Femtosecond laser ablation reduces this roughness but increases the manufacturing time. Microcantilevers fabricated by a focused ion beam are smooth and thin, although the fabrication process requires expensive equipment and long manufacturing times. In contrast to the reduction technology, the femtosecond laser-induced two-photon polymerization (TPP) three-dimensional (3D) nanoprinting technology is based on the manufacturing principle of layer-by-layer stacking, which greatly improves the flexibility and forming ability for microstructure designs.^{30,31} With the continuous development and improvement of the TPP 3D nanoprinting technology, the application of this technology has been greatly enriched and expanded, such as micro-optical devices, integrated optical devices, MEMS and biomedical devices, and other fields of application research. In 2018, Thompson *et al.*³² reported a microscale fiber-optic force sensor printed on fiber tip by TPP and realized a force resolution of 1.5 μN . In 2021, our group²⁰ reported a printed clamped-beam based fiber-optic force sensor and achieved a force resolution of 55 nN. In 2023, our group³⁰ proposed an optimized microcantilever based fiber-optic force sensor with a force resolution of 2.1 nN. With the growing maturity of and continuing improvements in the femtosecond laser-induced TPP 3D nanoprinting technology, mechanical metamaterials with

designable internal unit structures have opened the door to exploration of special structural mechanical properties. Therefore, it is expected to adjust and control the overall performances of mechanical metamaterials through the design of the internal structures of artificial construction units, thus greatly expanding the design space for new materials.^{33–35}

Herein, we combine the femtosecond laser-induced TPP 3D nanoprinting technology with mechanical metamaterials to fabricate the fiber end for a fiber-optic microforce sensor. The microcantilever beam constructed from the mechanical metamaterial shows good force sensitivity. The static mechanical properties of the proposed structure are analyzed by applying the finite element method (FEM) to the honeycomb structure of the cantilever beam. The elastic constant k of the fiber-optic microforce sensor can be adjusted by two orders of magnitude, from 0.165 to 46 N/m, and the cantilever geometry can be tailored to vary the mechanical properties of the probe and match the mechanical properties of relevant biological specimens. The resulting force resolution ranges down to 130 pN, which is much lower than the resolution of any other optical fiber microforce sensors reported to date. In addition, the optical fiber microforce sensor shows an ultra-high sensitivity of 154 nm/ μN and thus has immense potential for use in biomechanics and materials measurement applications.

II. RESULTS AND DISCUSSION

A. Sensing principles

The sensor uses optical fiber transmission rather than the complex optical rod path of atomic force microscopy (AFM) systems and acquires the signals via optical interference. As shown in Fig. 1(a), the FPI sensor consists of a silica glass insert, a single-mode fiber (SMF), and a microcantilever. The sensor design and fabrication details are presented in the supplementary material, S1 and S3. The reflection spectrum of the sensor shows three-beam interference formed by the resonance of the optical fiber end face, the lower surface of the microcantilever, and the upper surface of the microcantilever. An air microcavity (FPI1) with a length of L_{Air} is formed between the optical fiber end face and the lower surface of the microcantilever beam. A polymer microcavity (FPI2) with a length of L_{Poly} is formed between the upper and lower surfaces of the microcan-

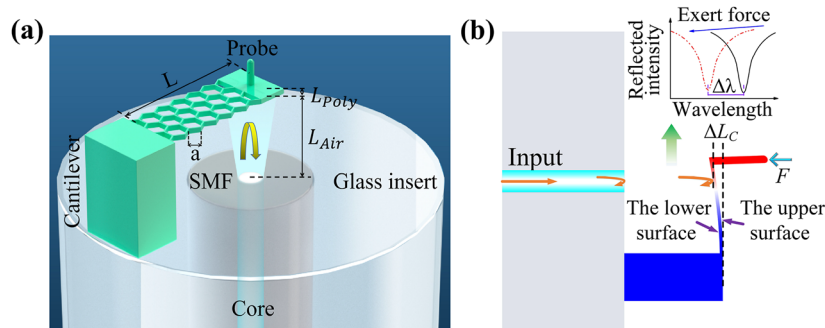


FIG. 1. (a) Schematic diagram of the all-fiber microforce sensor based on the fiber-optic microforce sensor. (b) Spectral schematic diagram for measuring applied external force.

tiler beam. Finally, a mixed microcavity (FPI3) with a length of $L_{Air} + L_{Poly}$ is formed between the optical fiber end face and the upper surface of the microcantilever beam. Here, the light intensity of FPI3 is relatively weak when compared with that of FPI1 and FPI2, and the light intensity of FPI2 is fixed after the cantilever beam is fabricated. Therefore, the change in the reflection spectrum is caused by the change in the FPI1 cavity of the air medium when a force is applied to the probe of the microcantilever beam. The free spectral range of FPI1 can be calculated using the following equation:³⁶

$$FSR = \frac{\lambda^2}{2nL_C}, \tag{1}$$

where λ is the resonant wavelength, L_C is the F-P cavity length, and n is the refractive index of the F-P cavity medium.

When the probe is subjected to a force, the microcantilever beam then bends and deforms, and the optical path difference in the F-P cavity changes together with the interference fringes. The bending degree of the microcantilever can be determined by detecting the resonant wavelength at the peak or trough in the interference spectrum. The corresponding relationship between the change in wavelength ($\Delta\lambda$) and the change in length of the F-P cavity (ΔL_C) can be simplified as follows:¹⁹

$$\frac{\Delta\lambda}{\lambda} = \frac{\Delta L_C}{L_C}. \tag{2}$$

The cavity length change can be inferred by monitoring the drift of the interference spectrum, and the external force exerted on the probe can then be measured, as shown in Fig. 1(b).

B. Design and simulation

Honeycomb is a magical product of nature, with the largest available space, which can minimize the amount of material used, thereby achieving minimum weight and showing great mechanical potential. The structure of the cantilever beam adopts the metamaterial of honeycomb structure. The metamaterial of honeycomb structure is a new type of porous topological material, which has the advantages of variable topological structure, high specific stiffness, and high resilience.^{37,38} By introducing it into the cantilever structure, the stiffness coefficient of the cantilever beam can be tuned in a wide range. By adopting the control variable method, the details of the microcantilever beam with a honeycomb structure are completely consistent except that the side length (a) and length of the cantilever beam (L) are different, as shown in Fig. 2. The cross-sectional area of the base under the cantilever beam is $60 \times 60 \mu\text{m}^2$, which can improve adhesion with the end face of the glass insert. By keeping the thickness to $5 \mu\text{m}$, the side length of the honeycomb cell in the microcantilever beam increases from 0.5 to $15 \mu\text{m}$ and the beam length increases from 60 to $200 \mu\text{m}$. The sensor design details are presented in the supplementary material, S1.

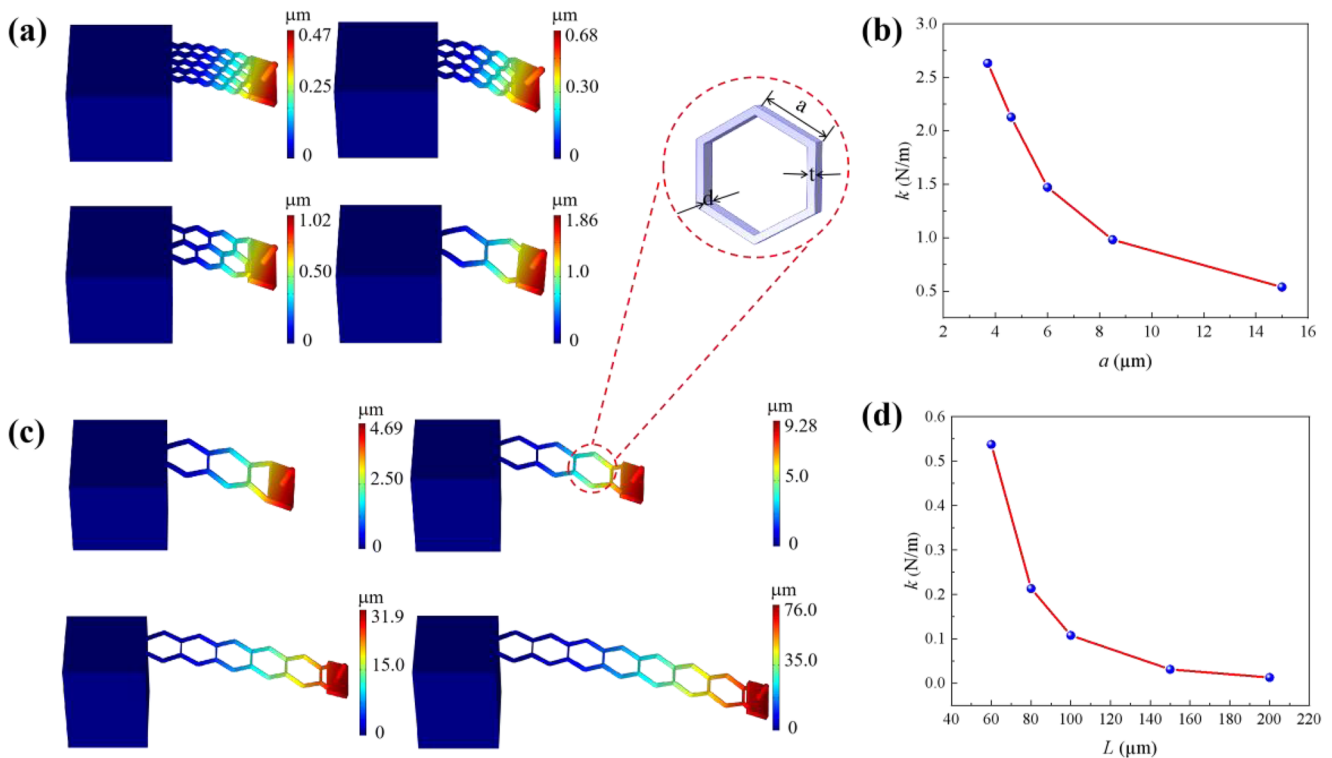


FIG. 2. (a) and (c) Finite-element analysis of the stress distributions of cellular microcantilever probes with the honeycomb cell side lengths a of 4.5, 6, 8.5, and 15 μm and microcantilever beam lengths L of 80, 100, 150, and 200 μm . (b) and (d) Relationship between a , L , and the elastic coefficient of the microcantilever.

The elastic constant k of the microcantilever beam is an important parameter of the probe because the uncertainty of k is one of the main sources of microforce measurement errors. The theoretical calculation formula for the elastic constant k of the microcantilever beam is as follows:³⁹

$$k = \frac{F}{d} = \frac{Ebt^3}{4L^3}, \quad (3)$$

where k (N/m) is the elastic constant of the microcantilever beam, F (N) is the point load on the end of the microcantilever beam, and d (m) is the deflection of the microcantilever beam. E (Pa) is Young's modulus of the microcantilever material, and L (m), b (m), and t (m) are the length, width, and thickness of the rectangular microcantilever beam, respectively.

To study the static mechanical properties of the honeycomb cantilever probe, the FEM is implemented to establish force sensor models with different structural parameters for the same stress, and the simulation results from this model are shown in Fig. 2. The material parameters, which include Young's modulus, the Poisson ratio, and the density of the polymer cantilever, are 2.34 GPa, 0.33, and 1499 kg m⁻³, respectively. A quantitative relationship is established between the microstructure size and the controllable elastic coefficient to predict the sensor size and guide preparation of the fiber-optic microforce sensor. The same microforce of 1 μN is applied to the probe, and the deformation of each area when subjected to this force is as shown in Figs. 2(a) and 2(c). The deformation increases with increasing honeycomb cell side length (a), and the deflection of the microcantilever beam is shown in Fig. 2(a). The relationship between a and the flexural elastic coefficient k of the cantilever beam, as illustrated in Fig. 2(b). Figure 2(c) shows that the deflection of the microcantilever beam increases with the length (L) of the cantilever beam, as shown in Fig. 2(d). The reason for this behavior is that a smaller side length (a) and smaller beam length (L) reduce the effective area of the cantilever beam. A smaller effective surface area for the cantilever beam enables greater flexural deformation and leads to higher sensitivity for the sensor. This result is consistent with the theoretical formula for a rectangular cantilever beam, which can provide theoretical guidance for the design of the required adjustment and control of the elastic coefficient k of the honeycomb cantilever beam. The illustration in Fig. 2(c) shows the parameters for each unit cell, as encircled by the red dotted line, including the edge width t , the edge length a , and the microcantilever thickness d . Because of the low stiffness of the polymeric materials used, the cantilever beam thickness d cannot be too small, and thus, a thickness of 5 μm was selected to ensure good support and high sensitivity for the cantilever beam. The edge width t of 0.5 μm was selected for the microcantilever beam structure in each of the following designs.

C. Characterization of the 3D printed mechanical metamaterial microcantilever

Figures 3(a)–3(h) show scanning electron microscopy (SEM) images of the microcantilever beam. Figures 3(a)–3(d) show the honeycomb cell lattices with side lengths of 4.5, 6, 8.5, and 15 μm, where the other parameters remain unchanged ($L = 60$ μm). When the honeycomb cell lattice side length is 15 μm, the beam lengths of microcantilever are 80, 100, 150, and 200 μm, as shown in Figs. 3(e)–3(h), respectively. The SEM images in Figs. 3(a)–3(h)

show that the actual microcantilever beam size remains consistent with the designed size. The structure basically consists of three parts. At the bottom, the sectional area of the base is 60 × 60 μm², and at the top, the microcantilever is attached to a base with a width of 30 μm and a thickness of 5 μm. Above the cuboid block (15 × 30 × 5 μm³) at the end of the microcantilever beam, a probe with a height of 15 μm and a diameter of 4 μm is located for use in mechanical testing. The top view shows that the surface is smooth and confirms that the shape is complete. The rectangular block located at the end of the microcantilever blocks the fiber core to stimulate interference.

To determine the mechanical properties of the fiber-optic microforce sensor, a nano-indenter (Hysitron TI980) is used. A cone tip (tip radius: 10 μm) of this nano-indenter pushes and pulls at the center of the probe at a constant speed of 400 nm/s. The effects of the side length of the honeycomb cell and the beam length on the mechanical properties of the microcantilever structure are studied. The honeycomb cell side length is increased from 0.5 to 15 μm initially, and as shown in Fig. 3(i), the force curves of six sets of microcantilevers show well-separated line shapes. Figure 3(g) shows that the elastic constant k ranges from 0.98 to 46 N/m. As can be seen in Fig. 3(i), the elastic constant k (46 N/m) is the highest and the displacement is the shortest when the honeycomb cell side length is 0.5 μm. The main reason is that the smaller the honeycomb cell side length, the larger the effective width of the microcantilever beam and the larger the elastic constant k . The k value of the microcantilever is related to the sensitivity, and a smaller k value indicates higher sensitivity. In fact, k can be adjusted by two orders of magnitude by varying the honeycomb cell side length a , and the mechanical properties of the microforce sensor can also be optimized by adjusting the length L to match the mechanical properties of biological samples. In the next step, L is increased from 60 to 200 μm, and as shown in Fig. 3(k), the elastic constant k decreases gradually with the length L when the size of hexagonal honeycomb elements in the microcantilever beams remains constant. Figure 3(l) shows that the first-order elastic constant k ranging from 0.165 to 0.98 N/m is also observed. It can be seen from Fig. 3(k) that the elastic constant k (0.98 N/m) is the highest and the displacement is the shortest when $L = 60$ μm. Furthermore, the smallest elastic constant k (0.165 N/m) is close to the minimum value for the AFM tip, and the range realized for the overall elastic constant k basically covers that of a typical commercial AFM probe.^{40,41} Finally, the stability of the microcantilever beam is evaluated by repeating the experiments above five times. Figures 3(m) and 3(n) show that the force curves of these five cycles overlap each other and that k remains constant (6.9 ± 0.2 N/m). The small fluctuations observed in the sensitivity confirm that the structure has excellent mechanical stability and resilience under compression conditions. All the k values are designated as linear fitted values for the structural compression process. Compared with the simulation results in Figs. 2(b) and 2(d), the k value measured in the experimental results is larger, which is mainly caused by the dimensional error of the preparation. This dimensional error is mainly caused by layer-by-layer printing and followed by structural shrinkage or deformation in development, which depends on the used laser power, scanning speed, surface tension of photoresist, and developer volatilization. Thus, these above fabrication parameters need to be repeatedly optimized to improve the printing quality.

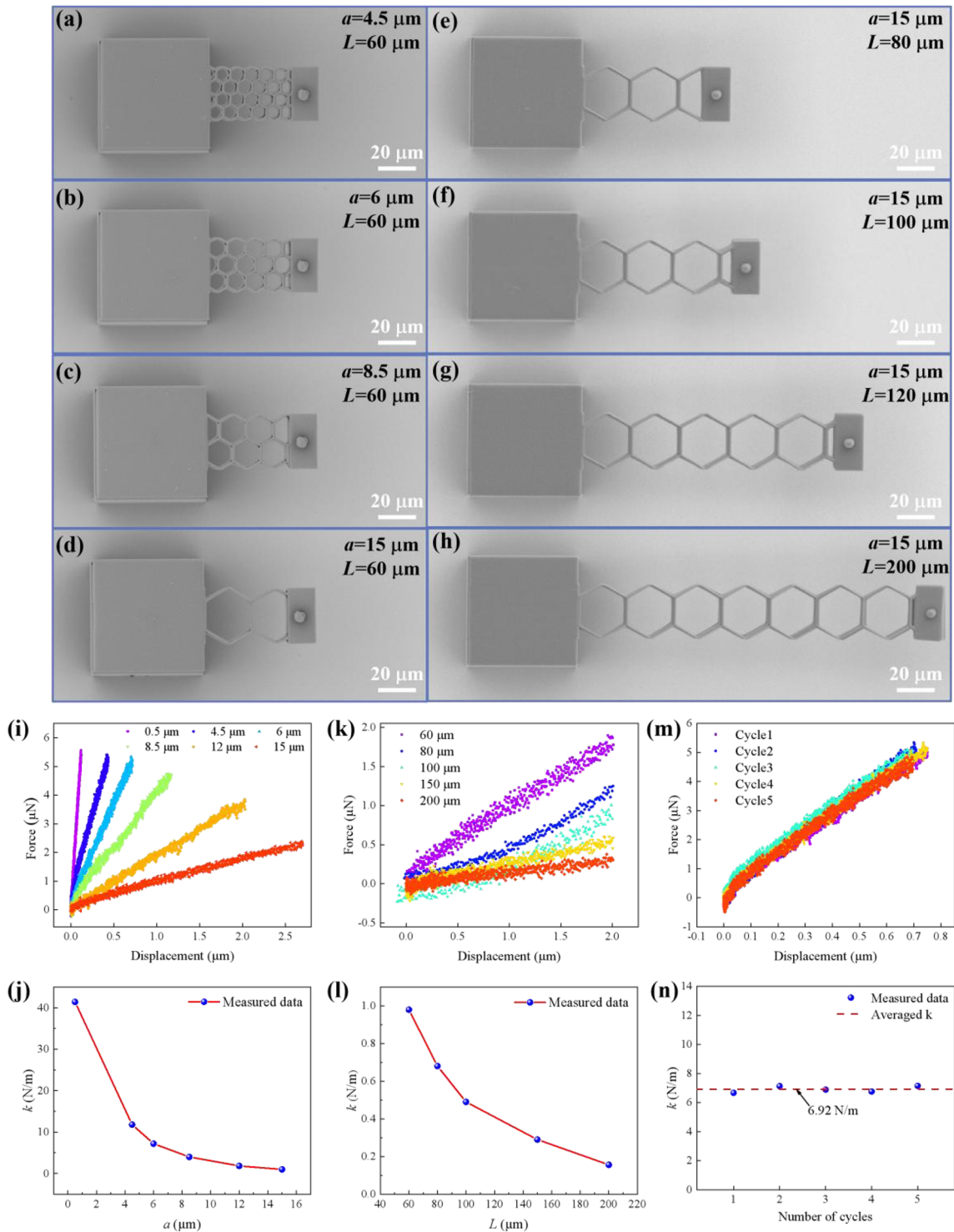


FIG. 3. (a)–(d) SEM images of microcantilever beams with the honeycomb cell side length a varying from 4.5 to 15 μm from top to bottom when $L = 60 \mu\text{m}$ and (e)–(h) with the beam length L varying from 80 to 200 μm when $a = 15 \mu\text{m}$. (i) The force–displacement curves (top) and (j) the elastic constant k (bottom) of microcantilever beams with the honeycomb cell side length a varying from 0.5 to 15 μm when $L = 60 \mu\text{m}$. (k) Force–displacement curves (top) and (l) the elastic constant k (bottom) for the microcantilevers with the beam length L varying from 60 to 200 μm when $a = 15 \mu\text{m}$. (m) Force–displacement curves were tested five times on the same cantilever beam ($a = 6 \mu\text{m}$, $L = 60 \mu\text{m}$). (n) The elastic constant k with an averaged 6.92 N/m.

20 September 2023 14:23:23

D. Force measurement

The elastic properties, optical properties, and mechanical properties of the probe are determined next. The elastic properties of the honeycomb cantilever probe were discussed earlier, and the cantilever probe with the lowest elastic coefficient k is analyzed here. The morphology of the probe was examined by SEM, as shown in Figs. 4(a)–4(c). The honeycomb cantilever probe on the optical fiber end face is clearly visible in these images, and its morphology is maintained. The sensor fabrication details are presented in the supplementary material, S3. Figures 4(a)–4(c) show the SEM images at different angles, and a smooth surface and parallelism between the optical fiber end face and the microcantilever can be observed. The structure used here improves the intensity of the reflected light and the sensitivity of the device to deformation.

Figure 4(d) shows the reflection spectrum of the microcantilever beams. The interference spectrum shows three-beam interference formed by the resonances of three mirrors on the fiber end face and on the upper and lower surfaces of the microcantilever beam. The small envelope within the spectrum is formed by the F–P cavity of the air medium, which contains the deflection information of the microcantilever beam to be monitored. The free spectral range of the

microcantilever near the wavelength of 1451.22 nm is 24.5 nm, and the extinction ratio is 9.6 dB. According to Eq. (1), the cavity length of the prepared microcantilever is $\sim 43 \mu\text{m}$.

According to Eq. (2), the microforce sensitivity can be obtained based on the interference spectrum shift caused by the unit force of the honeycomb cantilever probe. The device test system consists of a broadband source (BBS), an optical spectrum analyzer (OSA), a 3 dB coupler, and a 3D electric displacement platform for micro-manipulation, as shown in Fig. 5(b). A cover glass is placed on the sample holder, and the sensor probe is then placed on the cover glass surface such that the honeycomb structured cantilever beam deflects. The elastic coefficient k of the sensor probe is 0.165 N/m, as measured by *in situ* quantitative nano-indentation. The reaction force acting on the sensor probe is determined based on formula (3). Here, the elastic coefficient (k) of the microcantilever is 0.165 N/m, and the microcantilever probe is pressed with a phase-synchronous carry displacement each time, i.e., the bending deformation (d) of the microcantilever is 50 nm. According to Eq. (3), the microforce acting on the microcantilever beam is 8.25 nN at each step of 50 nm. During application of the progressive force, the reflection spectra are acquired in real time. Figure 5(a) shows the change in the reflection

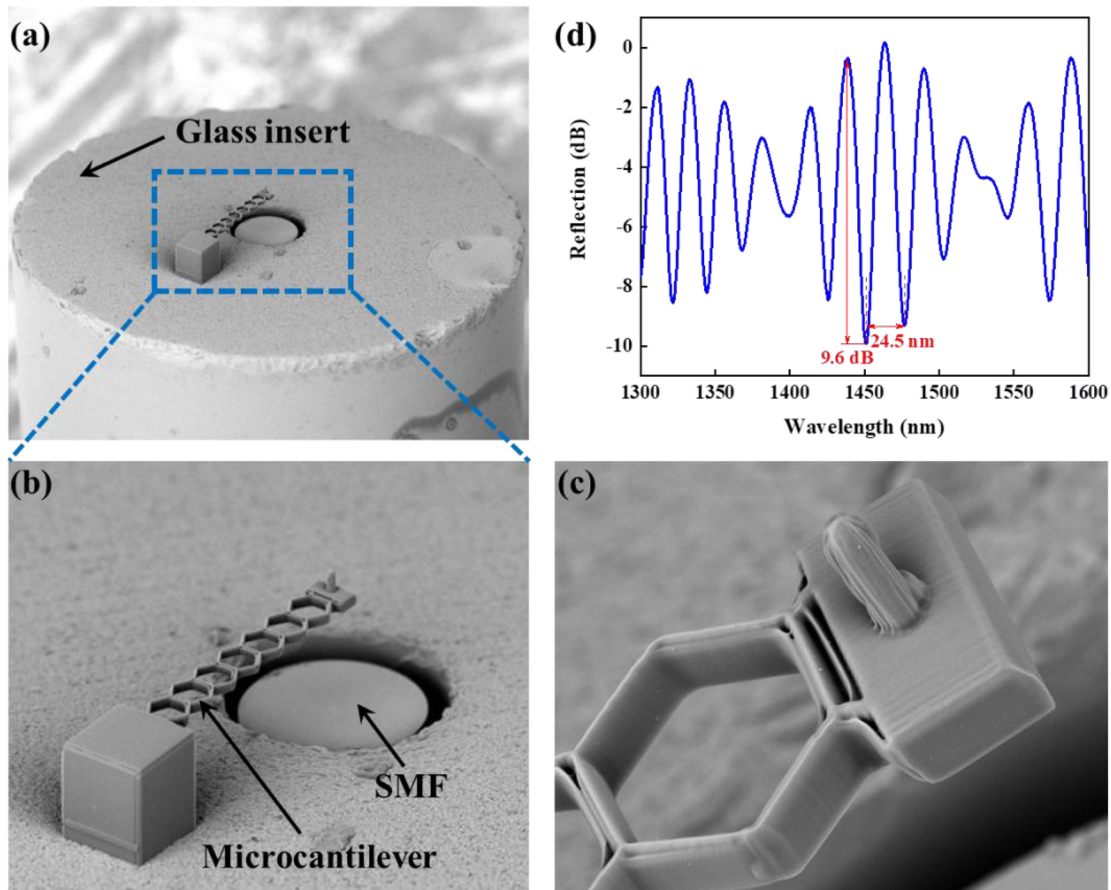


FIG. 4. (a)–(c) SEM images of the honeycomb cantilever probe and (d) reflection spectra of the honeycomb cantilever probe.

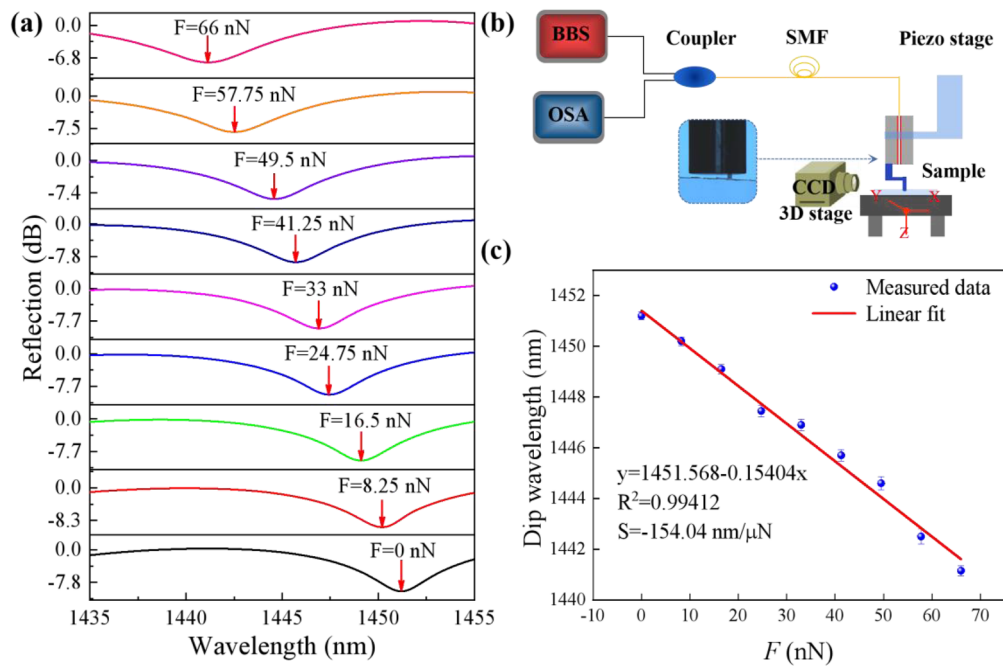


FIG. 5. (a) Reflection spectra of the sensor as the applied force is increased from 0 to 66 nN. (b) Measurement apparatus schematic and (c) linear fitting between the spectral variable and the force. The error bar represents the standard deviation for three repeated measurements.

spectrum when the force is increased gradually from 0 to 66 nN. A blue shift can be observed clearly at the tilted wavelength, as indicated by the arrow. The extinction ratio of the reflection spectrum decreases with increasing force because of the bending action of the cantilever beam. The relationship between the dip wavelength and the force is shown in Fig. 5(c). The force exerted on the cantilever is translated into the spectral shift of the light reflection minima in the fiber tip. As the applied force increases, the interference spectrum shifts toward the left. Based on linear fitting of the dip wavelength change, the force sensitivity is calculated to be 154 nm/ μ N. The

resolution of the force sensor is 130 pN under the limited resolution of 0.02 nm of the OSA.^{42–44} In the microforce sensing measurement regime, the sensor probe works within the framework of the linear elastic range, and there exists no lag between the force and the change in the cavity length.

As shown in Table I, when compared with previous optical fiber sensors, the optical fiber sensor described in this paper shows superior sensitivity and other advantages that include flexible manufacturing capability, high mechanical strength, and ultra-low force resolution. The resulting force resolution ranges down to 130 pN, which is much lower than that reported previously for any other optical fiber microforce sensors. The proposed optical fiber force sensor is applicable to measurement of weak forces of the order of piconewtons (pN) for biological samples.

TABLE I. Performance comparison of different optical fiber force sensors.

Sensor structure	Force sensitivity (nm/ μ N)	Resolution (nN)	Reference
SPR-POF	4.4×10^{-6}	2.2×10^7	45
FP micro-cavity	3×10^{-6}	3.4×10^5	46
LPG	5.14×10^{-3}	1.56×10^4	47
SiO ₂ FPI	0.36	6×10^2	48
FTMS FPI	1.05	19	49
Clamped beam probe fiber FPI	1.51	55	20
PDMS fiber FPI	45.72	0.44	50
FONP	54.5	2.1	30
Microcantilever FPI	154	0.13	This work

III. CONCLUSION

Femtosecond laser-induced TPP 3D nanoprinting technique is designed to print a fiber-optic microforce sensor on the end face of a single-mode fiber with a glass insert. The elastic constant k of the fabricated fiber-optic microforce sensor can be adjusted by two orders of magnitude from 0.165 to 46 N/m, and the geometric configuration of the cantilever beam can be tailored to match the mechanical properties of biological specimens. The all-fiber microforce sensor shows an ultra-high force sensitivity of 154 nm/ μ N and an ultra-low force resolution of 130 pN; these values are superior to those reported recently for similar optical fiber force sensors. Because of the flexibility of the polymeric materials used, the sensor shows

excellent stability and repeatability over multiple mechanical cycles. The proposed sensor boasts advantages that include simple manufacturing, high sensitivity, high flexibility, and reproducibility, and it has excellent prospects for use in biomechanical detection.

SUPPLEMENTARY MATERIAL

See the supplementary material for the design and simulation and the materials and methods.

ACKNOWLEDGMENTS

This work was supported by the Shenzhen Science and Technology Program (Grant No. RCYX20200714114524139), Shenzhen Key Laboratory of Ultrafast Laser Micro/Nano Manufacturing (Grant Nos. ZDSYS20220606100405013 and JCYJ20200109114001806), the Science and Technology Innovation Commission of Shenzhen (Grant No. JSGG20201102152200001), the Natural Science Foundation of Guangdong Province (Grant Nos. 2022B1515120061 and 2022A1515110971), the National Natural Science Foundation of China (Grant Nos. 62122057, 62075136, 62105217, and 62305223), and the China Postdoctoral Science Foundation (Grant No. 2022M722173).

AUTHOR DECLARATIONS

Conflict of Interest

The authors have no conflicts to disclose.

Author Contributions

F.W. and M.Z. contributed equally to this work.

Famei Wang: Conceptualization (equal); Data curation (equal); Formal analysis (equal); Funding acquisition (equal); Investigation (equal); Software (equal); Validation (equal); Visualization (equal); Writing – original draft (equal). **Mengqiang Zou:** Conceptualization (equal); Resources (equal); Supervision (equal); Writing – original draft (equal); Writing – review & editing (supporting). **Changrui Liao:** Conceptualization (equal); Funding acquisition (equal); Project administration (equal); Resources (equal); Supervision (equal); Writing – original draft (equal); Writing – review & editing (supporting). **Bozhe Li:** Investigation (supporting); Software (supporting). **Dejun Liu:** Writing – review & editing (supporting). **Jie Zhou:** Data curation (supporting); Writing – review & editing (supporting). **Haoqiang Huang:** Investigation (supporting); Writing – review & editing (supporting). **Jinlai Zhao:** Investigation (supporting); Software (supporting). **Chao Liu:** Supervision (supporting); Writing – review & editing (supporting). **Paul K. Chu:** Writing – review & editing (supporting). **Yiping Wang:** Conceptualization (supporting); Funding acquisition (supporting); Project administration (supporting); Writing – review & editing (equal).

DATA AVAILABILITY

The data that support the findings of this study are available from the corresponding authors upon reasonable request.

REFERENCES

- P. Nautiyal, F. Alam, K. Balani, and A. Agarwal, "The role of nanomechanics in healthcare," *Adv. Healthcare Mater.* **7**, 1700793 (2018).
- D. J. Sirebuly, R. W. Friddle, J. Villanueva, and Q. Huang, "Nanomechanical force transducers for biomolecular and intracellular measurements: Is there room to shrink and why do it?," *Rep. Prog. Phys.* **78**, 024101 (2015).
- Q. Huang, J. Lee, F. T. Arce, I. Yoon, P. Angsantikul, J. Liu, and Y. S. Shi, "Nanofibre optic force transducers with sub-piconewton resolution via near-field plasmon-dielectric interactions," *Nat. Photonics* **11**, 352–355 (2017).
- K. C. Neuman and A. Nagy, "Single-molecule force spectroscopy: Optical tweezers, magnetic tweezers and atomic force microscopy," *Nat. Methods* **5**, 491–505 (2008).
- S. E. Cross, Y.-S. Jin, J. Tondre, R. Wong, J. Rao, and J. K. Gimzewski, "AFM-based analysis of human metastatic cancer cells," *Nanotechnology* **19**, 384003 (2008).
- S. Suresh, "Biomechanics and biophysics of cancer cells," *Acta Mater.* **55**, 3989–4014 (2007).
- G. Zhang, M. Long, Z. Z. Wu, and W. Q. Yu, "Mechanical properties of hepatocellular carcinoma cells," *World J. Gastroenterol.* **8**, 243 (2002).
- C. R. Liao, C. Xiong, J. L. Zhao, M. Q. Zou, Y. Y. Zhao, B. Z. Li, P. Ji, Z. H. Cai, Z. S. Gan, Y. Wang, and Y. P. Wang, "Design and realization of 3D printed fiber-tip microcantilever probes applied to hydrogen sensing," *Light: Adv. Manuf.* **3**, 3 (2022).
- C. Deufel, S. Forth, C. R. Simmons, S. Dejgosh, and M. D. Wang, "Nanofabricated quartz cylinders for angular trapping: DNA supercoiling torque detection," *Nat. Methods* **4**, 223–225 (2007).
- F. Alam and K. Balani, "Adhesion force of staphylococcus aureus on various biomaterial surfaces," *J. Mech. Behav. Biomed. Mater.* **65**, 872 (2017).
- G. Thalhammer, R. Steiger, S. Bernet, and M. R. Marte, "Optical macro-tweezers: Trapping of highly motile micro-organisms," *J. Opt.* **13**, 044024 (2011).
- M. Dong, S. Husale, and O. Sahin, "Determination of protein structural flexibility by microsecond force spectroscopy," *Nat. Nanotechnol.* **4**, 514 (2009).
- T. Sanuki, M. Tano, W. Gao, and S. Kiyono, "Design and construct of a long-stroke fast-tool-servo equipped with a force sensor (Nano/micro measurement and intelligent instrument)," in *Proceedings of International Conference on Leading Edge Manufacturing in 21st Century LEM21* (The Japan Society of Mechanical Engineers, 2005), Vol. 2, pp. 357–360.
- B. Deng, L. Zhou, F. Y. Peng, R. Yan, M. H. Yang, and M. Liu, "Analytical model of cutting force in micromilling of particle-reinforced metal matrix composites considering interface failure," *J. Manuf. Sci. Eng.* **140**, 081009 (2018).
- T. Gissibl, S. Thiele, A. Herkommer, and H. Giessen, "Sub-micrometre accurate free-form optics by three-dimensional printing on single-mode fibres," *Nat. Commun.* **7**, 11763 (2016).
- T. Gissibl, S. Thiele, A. Herkommer, and H. Giessen, "Two-photon direct laser writing of ultracompact multi-lens objectives," *Nat. Photonics* **10**, 554–560 (2016).
- M. H. Wang, K. H. Zhao, J. Y. Wu, Y. Q. Li, Y. Yang, S. Huang, J. R. Zhao, and K. P. Chen, "Femtosecond laser fabrication of nanograting-based distributed fiber sensors for extreme environmental applications," *Int. J. Extreme Manuf.* **3**, 025401 (2021).
- J. Q. Huang, L. A. Blanquer, J. Bonafacio, E. R. Logan, D. A. D. Corte, and J. M. Tarascon, "Operando decoding of chemical and thermal events in commercial Na(Li)-ion cells via optical sensors," *Nat. Energy* **5**, 674–683 (2020).
- C. Xiong, J. T. Zhou, C. R. Liao, M. Zhu, Y. Wang, and Y. P. Wang, "Fiber-tip polymer microcantilever for fast and highly sensitive hydrogen measurement," *ACS Appl. Mater. Interfaces* **12**, 33163–33172 (2020).
- M. Q. Zou, C. R. Liao, S. Liu, C. Xiong, C. Zhao, J. Zhao, Z. S. Gan, Y. Chen, K. Yang, and D. Liu, "Fiber-tip polymer clamped-beam probe for high-sensitivity nanoforce measurements," *Light: Sci. Appl.* **10**, 171 (2021).
- D. Iannuzzi, S. Deladi, J. V. Gadgil, R. G. P. Sanders, and H. Schreuders, "Monolithic fiber-top sensor for critical environments and standard applications," *Appl. Phys. Lett.* **88**, 053501 (2006).
- M. Cui, C. H. Van Hoorn, and D. Iannuzzi, "Miniaturized fibre-top cantilevers on etched fibres," *J. Microsc.* **264**, 370–374 (2016).

- ²³S. Hamad, G. K. Podagatlapalli, R. Mounika, S. V. S. Nageswara Rao, and A. P. Pathak, "Studies on linear, nonlinear optical and excited state dynamics of silicon nanoparticles prepared by picosecond laser ablation," *AIP Adv.* **5**, 127127 (2015).
- ²⁴H. Zhang and Z. Bai, "Optical fiber end-pumped high energy picosecond laser," *Appl. Laser* **38**, 119–122 (2018).
- ²⁵L. L. Liu, Y. Q. Ren, M. Wang, and M. Zou, "Optical fiber Fabry-Perot interferometer sensor fabricated by femtosecond laser-induced water breakdown," *Integr. Ferroelectr.* **208**, 55–59 (2020).
- ²⁶K. Sloyan, H. Melkonyan, H. Apostoleris, M. Dahlem, M. Chiesa, and A. Al Ghaferi, "A review of focused ion beam applications in optical fibers," *Nanotechnology* **32**, 472004 (2021).
- ²⁷C. Holmes, A. Jantzen, A. C. Gray, L. G. Carpenter, and P. G. R. Smith, "Integrated optical fiber-tip cantilevers," *IEEE Sens. J.* **17**, 6960–6965 (2017).
- ²⁸D. Chavan, G. Gruca, T. V. D. Watering, K. Heeck, J. Rector, M. Slaman, D. Andres, B. Tiribilli, G. Margheri, and D. Iannuzzi, "Fiber-top and ferrule-top cantilevers for atomic force microscopy and scanning near field optical microscopy," *Proc. SPIE* **8430**, 84300Z (2012).
- ²⁹D. Chavan, D. Andres, and D. Iannuzzi, "Note: Ferrule-top atomic force microscope. II. Imaging in tapping mode and at low temperature," *Rev. Sci. Instrum.* **82**, 046107 (2011).
- ³⁰M. Q. Zou, C. R. Liao, Y. P. Chen, L. Xu, S. Tang, G. X. Xu, K. Ma, J. T. Zhou, Z. H. Cai, B. Z. Li, C. Zhao, Z. R. Xu, Y. Y. Shen, S. Liu, Y. Wang, Z. S. Gan, H. Wang, X. M. Zhang, S. Kasas, and Y. P. Wang, "3D printed fiber-optic nanomechanical bioprobe," *Int. J. Extreme Manuf.* **5**, 015005 (2023).
- ³¹D. W. Zhang, H. M. Wei, H. Z. Hu, and S. Krishnaswamy, "Highly sensitive magnetic field microsensors based on direct laser writing of fiber-tip optofluidic Fabry-Pérot cavity," *APL Photonics* **5**, 076112 (2020).
- ³²A. J. Thompson, M. Power, and G. Yang, "Micro-scale fiber-optic force sensor fabricated using direct laser writing and calibrated using machine learning," *Opt. Express* **26**, 14186–14200 (2018).
- ³³J. C. Sanger, B. R. Pauw, B. Riechers, A. Zocca, J. Rosalie, R. Maaß, H. Sturm, and J. Gunster, "Entering a new dimension in powder processing for advanced ceramics shaping," *Adv. Mater.* **35**, 2208653 (2022).
- ³⁴C. Xiong, C. R. Liao, Z. Y. Li, K. M. Yang, M. Zhu, Y. Y. Zhao, and Y. P. Wang, "Optical fiber integrated functional micro-/nanostructure induced by two-photon polymerization," *Front. Mater.* **7**, 586496 (2020).
- ³⁵M. H. Fu, F. M. Liu, and L. L. Hu, "A novel category of 3D chiral material with negative Poisson's ratio," *Compos. Sci. Technol.* **160**, 111–118 (2018).
- ³⁶Z. Y. Li, C. R. Liao, J. Wang, Z. L. Li, P. Zhou, Y. Wang, and Y. P. Wang, "Femtosecond laser microprinting of a fiber whispering gallery mode resonator for highly-sensitive temperature measurements," *J. Lightwave Technol.* **37**, 1241–1245 (2019).
- ³⁷Q. C. Zhang, X. H. Yang, P. Li, G. Y. Huang, S. S. Feng, C. Shen, B. Han, X. H. Zhang, F. Jin, F. Xu, and T. J. Lu, "Bioinspired engineering of honeycomb structure—Using nature to inspire human innovation," *Prog. Mater. Sci.* **74**, 332–400 (2015).
- ³⁸W. Jiang, L. L. Yan, H. Ma, Y. Fan, J. F. Wang, M. D. Feng, and S. B. Qu, "Electromagnetic wave absorption and compressive behavior of a three-dimensional metamaterial absorber based on 3D printed honeycomb," *Sci. Rep.* **8**, 4817 (2018).
- ³⁹R. Li, H. F. Ye, W. S. Zhang, G. J. Ma, and Y. W. Su, "An analytic model for accurate spring constant calibration of rectangular atomic force microscope cantilevers," *Sci. Rep.* **5**, 15828 (2015).
- ⁴⁰K. Q. Chen and W. G. Xie, "Choice of AFM probe and solution of some abnormal phenomena," *Res. Explor. Lab.* **33**, 19–22 (2014).
- ⁴¹Y. Hao, S. Cheng, Y. Tanaka, Y. Hosokawa, Y. Yalikun, and M. Li, "Mechanical properties of single cells: Measurement methods and applications," *Biotechnol. Adv.* **45**, 107648 (2020).
- ⁴²Q. Liu, L. Xing, Z. X. Wu, L. Cai, Z. R. Zhang, and J. C. Zhao, "High-sensitivity photonic crystal fiber force sensor based on Sagnac interferometer for weighing," *Opt. Laser Technol.* **123**, 105939 (2020).
- ⁴³P. Ji, M. Zhu, C. R. Liao, C. Zhao, K. M. Yang, C. Xiong, and Y. Wang, "In-fiber polymer microdisk resonator and its sensing applications of temperature and humidity," *ACS Appl. Mater. Interfaces* **13**, 48119–48126 (2021).
- ⁴⁴C. X. Li, Y. Liu, C. P. Lang, Y. L. Zhang, and S. L. Qu, "Femtosecond laser direct writing of a 3D microcantilever on the tip of an optical fiber sensor for on-chip optofluidic sensing," *Lab Chip* **22**, 3734–3743 (2022).
- ⁴⁵F. Arcadio, L. Zeni, and N. Cennamo, "Exploiting plasmonic phenomena in polymer optical fibers to realize a force sensor," *Sensors* **22**, 2391 (2022).
- ⁴⁶O. R. Ranjbar-Naeni, F. Jafari, P. Zarafshani, M. I. Zibaii, and H. Latifi, "Design and fabrication of micro silica sphere cavity force sensor based on hybrid Fabry Perot interferometer," *Proc. SPIE* **10329**, 1032936 (2017).
- ⁴⁷W. S. J. Ferreira, P. S. S. dos Santos, P. Caldas, P. A. S. Jorge, and J. M. S. Sakamoto, "Micro-force measurement with pre-curvature long-period fiber grating-based sensor," *EPJ Web Conf.* **238**, 12009 (2020).
- ⁴⁸S. Pevec and D. Donlagic, "Miniature all-fiber force sensor," *Opt. Lett.* **45**(18), 5093–5096 (2020).
- ⁴⁹M. Q. Zou, C. R. Liao, Y. P. Chen, Z. S. Gan, S. Liu, D. J. Liu, L. Liu, and Y. P. Wang, "Measurement of interfacial adhesion force with a 3D-printed fiber-tip microforce sensor," *Biosensors* **12**, 629 (2022).
- ⁵⁰W. J. Bao, X. Y. Li, F. Y. Chen, R. H. Wang, and X. G. Qiao, "Hyperelastic polymer fiber Fabry-Pérot interferometer for nanoforce measurement," *J. Lightwave Technol.* **40**(12), 4020–4026 (2022).